SU(3) Quantum Hall Ferromagnetism in SnTe

Xiao Li (李潇),[1] Fan Zhang,[3,*] and A. H. MacDonald[2]
[1]Condensed Matter Theory Center and Joint Quantum Institute, University of Maryland, College Park, Maryland 20742, USA
[2]Department of Physics, The University of Texas at Austin, Austin, Texas 78712, USA
[3]Department of Physics, The University of Texas at Dallas, Richardson, Texas 75080, USA
(Received 12 July 2015; published 15 January 2016)

The (111) surface of SnTe hosts one isotropic $\bar{\Gamma}$-centered and three degenerate anisotropic $\bar{M}$-centered Dirac surface states. We predict that a nematic phase with spontaneously broken $\mathcal{C}_3$ symmetry will occur in the presence of a perpendicular magnetic field when the $N = 0$ $\bar{M}$ Landau levels are $1/3$ or $2/3$ filled. The nematic state phase boundary is controlled by a competition between intravalley Coulomb interactions that favor a valley-polarized state and weaker intervalley scattering processes that increase in relative strength with magnetic field. An in-plane Zeeman field alters the phase diagram by lifting the threefold $\bar{M}$ Landau-level degeneracy, yielding a ground state energy with $2\pi/3$ periodicity as a function of Zeeman-field orientation angle.

DOI: 10.1103/PhysRevLett.116.026803

Introduction.—Tin telluride (SnTe) is now attracting great attention as the first topological insulator (TI) protected purely by crystalline symmetry. Although its electronic band structure has been understood [1] for decades, the physical consequences of its band inversion have only recently been fully appreciated [2]. SnTe has a rocksalt crystal structure with two interpenetrating face-centered cubic lattices, and bulk bands that are inverted at the four Brillouin-zone boundary L points. Its mirror Chern number becomes nontrivial in mirror-invariant planes that each contain a pair of L points. Based on this property, Dirac surface states on selected surfaces respecting mirror symmetries were first predicted [2] and later observed [3–5]. The (111) surface of SnTe [6–13] respects three mirror symmetries, and each protects an anisotropic gapless Dirac surface state at $\bar{M}$ and a partner isotropic state at $\bar{\Gamma}$ in the surface Brillouin zone, as sketched in Fig. 1(a).

In crystalline topological insulators the top and bottom surfaces of thin films can be electrically isolated [8] by breaking mirror symmetries on the side surfaces while leaving them time-reversal invariant. This behavior contrasts with the case of strong TI thin films, for which it is impossible to study single surface electrical properties because sidewalls can be gapped only by breaking time-reversal symmetry and generating Hall currents [14]. The (111) surface of SnTe therefore hosts a unique and relatively unexplored isolated two-dimensional electron gas (2DEG) system in which the interplay between topological surface properties, valleytronics, and many-body effects is likely to yield unexpected phenomena.

The integer quantum Hall (QH) effect is a hallmark of any 2DEG system. When a 2DEG has Landau-level (LL) degeneracies due to spin, valley, and/or layer degrees of freedom [15–17], the interplay between Landau quantization and electron-electron interactions often leads to ground states in which symmetries associated with the aforementioned degrees of freedom are spontaneously broken. Examples of broken symmetry states of this type, often referred to as QH ferromagnets, arise in GaAs and AlAs quantum wells [18,19], single- and multilayer graphene sheets [20–23], and on the surfaces of silicon [24,25] and bismuth [26,27]. In all instances of QH ferromagnetism studied to date, however, the noninteracting LL degeneracy N has always been even. Thus, one may wonder whether QH ferromagnetism with odd N exists in some material, and how in this case the ground state breaks Hamiltonian symmetries.

Here, we show that the (111) surface of SnTe provides a platform to explore SU(3) QH ferromagnetism. As illustrated in Fig. 1, the four Dirac cones on the (111)

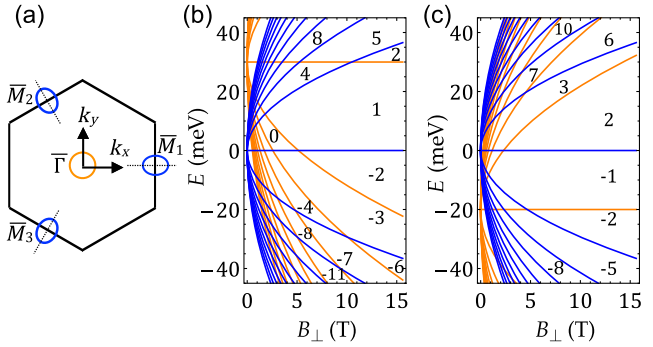

FIG. 1. (a) Typical equal-energy contours for gapless Dirac states on the (111) surface of SnTe. The three mirror invariance lines are indicated by dotted lines. (b),(c) Single-particle LL structures of (a). The energy difference between $\bar{\Gamma}$ and $\bar{M}$ Dirac points is 30 meV in (b) and −20 meV in (c). Brown and blue lines represent the nondegenerate $\bar{\Gamma}$ LLs and the threefold degenerate $\bar{M}$ LLs, respectively. The integer labels in (b) and (c) give LL filling factors in spectral gaps.

surface give rise to four LL sequences. The three $\bar{M}$ LL sequences are degenerate and related by a $\mathcal{C}_3$ rotational symmetry. However, the $\bar{\Gamma}$-$\bar{M}$ LL energy difference is not restricted by any symmetry and can be tuned [11]. Thus, there will be field-dependent LL crossings between different groups of LLs. We focus here on the case in which the $N = 0$ triplet is at the Fermi energy, well separated from all $\bar{\Gamma}$ LLs, and 1/3 or 2/3 filled to yield an integer total filling factor. This triplet has an exact SU(3) flavor symmetry in the absence of interactions and Zeeman fields, which is a consequence of the $\mathcal{C}_3$ symmetry of the crystal and is analogous to the SU(3) flavor symmetry of the quark model and the eightfold way. We find that when only the valley-conserving Coulomb interactions are retained in the theory, valley symmetry is spontaneously broken to create a nematic state [28] in which only one valley is occupied. When the weaker valley-exchange scattering processes are retained, a broken translational symmetry state with coherence among three valleys appears beyond a critical magnetic field strength. An in-plane Zeeman field couples to the nematic order parameter and influences the competition between broken rotational and translational symmetry states.

Surface state LLs.—The SnTe (111) Dirac surface states are described by the $\boldsymbol{k}\cdot\boldsymbol{p}$ Hamiltonians [8]

$$H_{\bar{\Gamma}} = \hbar v(k_x s_y - k_y s_x),$$
$$H_{\bar{M}_\lambda} = \hbar v_x k_x^{(\lambda)} s_y - v k_y^{(\lambda)} s_x, \tag{1}$$

where $v = 4.40 \times 10^5$ m/s and $v_x = 2.55 \times 10^5$ m/s [11] are surface Fermi velocities, $\lambda = 1, 2, 3$ labels the three inequivalent $\bar{M}$ valleys, and $\boldsymbol{s}$ is a surface Dirac pseudospin. Microscopically, the pseudospins [8,29] are valley-dependent linear combinations of spin and orbital operators that transform like spin under time reversal, spatial inversion, and mirror reflection. $k_x^{(\lambda)}$ and $k_y^{(\lambda)}$ are explicitly defined in Fig. 1(a) for the $\bar{M}_1$ valley; local momentum-space coordinates in other valleys are obtained by appropriate $\mathcal{C}_3$ rotations.

In the presence of a uniform perpendicular magnetic field, the 2D kinetic momenta $\hbar\boldsymbol{k}$ in Eq. (1) are replaced by $\boldsymbol{\pi} = \hbar\boldsymbol{k} + e\boldsymbol{A}$, where $\boldsymbol{A} = (0, -B_\perp x)$. The $\bar{\Gamma}$ LL energies are $E_{N,\pm}(\bar{\Gamma}) = \pm\sqrt{2\hbar v^2 NeB_\perp}$, reminiscent of the massless Dirac fermion LLs in graphene. Because the $\bar{M}$ surface states have anisotropic dispersions with valley-dependent orientations, we define the valley-dependent raising operators $a_\lambda^\dagger = (\ell/\sqrt{2}\hbar)(\alpha_\lambda \pi_x - i\beta_\lambda \pi_y)$, where $\ell = \sqrt{\hbar/eB_\perp}$ is the magnetic length, $\alpha_\lambda = \eta\cos\theta_\lambda + i\eta^{-1}\sin\theta_\lambda$, $\beta_\lambda = \eta^{-1}\cos\theta_\lambda + i\eta\sin\theta_\lambda$, $\eta = \sqrt{v_x/v}$, and $\theta_\lambda = 2(\lambda-1)\pi/3$. With these definitions,

$$H_{\bar{M}_\lambda} = \frac{\sqrt{2vv_x}\hbar}{\ell}\begin{pmatrix} 0 & -ia_\lambda^\dagger \\ ia_\lambda & 0 \end{pmatrix}, \tag{2}$$

so that the $\bar{M}$ LL energies and wave functions are $E_{N,\pm}(\bar{M}_\lambda) = \pm\sqrt{2\hbar v_x v N e B_\perp}$, and

$$\psi_{0\lambda} = \begin{pmatrix} \phi_{0\lambda} \\ 0 \end{pmatrix},$$
$$\psi_{N>0,\lambda,\pm} = \frac{1}{\sqrt{2}}\begin{pmatrix} \phi_{N\lambda} \\ \pm\frac{\alpha_\lambda^*}{|\alpha_\lambda|}\phi_{N-1,\lambda} \end{pmatrix}, \tag{3}$$

where

$$\phi_{N\lambda} = \mathcal{A}_{N\lambda}^{-1} e^{-\alpha_\lambda\beta_\lambda^*\xi_\lambda^2/2} H_N(\xi_\lambda). \tag{4}$$

Here, $\mathcal{A}_{N\lambda} = (2^N N!\sqrt{\pi}|\alpha_\lambda|\ell)^{1/2}$ is a normalization factor, $\xi_\lambda = (x - k_y\ell^2)/(|\alpha_\lambda|\ell)$, and $H_N(\xi)$ is the Hermite polynomial. Also, note that $a\phi_N = -i\alpha^*/|\alpha|\sqrt{N}\phi_{N-1}$ and $a\phi_0 = 0$. In Fig. 1 we plot LL spectra as a function of $B_\perp$ for cases with the $\bar{\Gamma}$ Dirac point above and below the $\bar{M}$ Dirac points. All of the $\bar{\Gamma}$ LLs are nondegenerate, whereas all of the $\bar{M}$ LLs are threefold degenerate because of the $\mathcal{C}_3$ symmetry.

QH ferromagnetism of $N = 0$ triplet.—We focus here on the case in which the $N = 0$ LL triplet is 1/3 or 2/3 filled, and we ask whether Hamiltonian symmetries are spontaneously broken and whether broken symmetries give rise to charged excitation gaps which would yield an integer QH effect. Because Coulomb interaction matrix elements are sensitive to the valley-dependent orientations of the anisotropic cyclotron orbits, the Hamiltonian is not invariant under rotations in valley space. However, the small size of the momentum-space cyclotron orbits relative to their separation implies that the number of electrons in each pocket is conserved; the only allowed large-momentum transfer processes simply exchange electrons between valleys. Broken symmetry ground states are either Ising-like states in which the three symmetry equivalent valleys are occupied by different numbers of electrons, or XY-like states in which coherence is spontaneously established among the valleys. The Ising-like state is a nematic [28], which lowers rotational symmetry, while the XY-like state is a commensurate charge-density-wave state which breaks the crystal translational symmetry. Interesting new physics is most likely to be experimentally accessible when the $N = 0$ triplet is partially filled because of the large gap separating $N = 0$ and $N \neq 0$ LLs. After projecting to the $N = 0$ triplet, states at 1/3 and 2/3 fillings are related by particle-hole symmetry within the triplet, allowing us to focus on the 1/3 case. We neglect the possibility of an accidental degeneracy between the $N = 0$ $\bar{M}$ triplet and the $\bar{\Gamma}$ LL.

We employ the unrestricted Hartree-Fock (HF) approximation [30] at the integer total filling factors of interest, and we minimize the energy of single Slater determinant trial wave functions by solving self-consistent field equations with 3×3 mean-field Hamiltonians of the form

$$\mathcal{H}^{\mathrm{HF}}_{\lambda\sigma} = E_0\delta_{\lambda\sigma} + Y_0^{\lambda\sigma}\Delta_{\sigma\lambda}(1-\delta_{\lambda\sigma}) - X_0^{\lambda\sigma}\Delta_{\sigma\lambda} - \sum_{\tau\neq\lambda} Z_0^{\lambda\tau}\Delta_{\tau\tau}\delta_{\lambda\sigma}, \quad (5)$$

where E_0 is the single-particle LL energy and $\Delta_{\sigma\lambda} = \langle c^\dagger_\sigma c_\lambda\rangle$ is the triplet density matrix. $X_0^{\lambda\sigma}$, $Y_0^{\lambda\sigma}$, and $Z_0^{\lambda\tau}$ are, respectively, intravalley exchange, intervalley Hartree, and intervalley exchange integrals. We use an envelope-function approximation for valley-conserving scattering processes, which are enhanced by the long-range tail of the Coulomb interactions and are therefore dominant, and we approximate intervalley processes using a phenomenological interaction constant $U \sim 2\pi e^2/\epsilon K$, where $\boldsymbol{K}$ is a primitive reciprocal lattice vector. It follows that the Hartree integral is $Y_0^{\lambda\sigma} = (2\pi\ell^2)^{-1}UF_{00}^{\lambda\sigma}(0)F_{00}^{\sigma\lambda}(0)$, and that the exchange integrals are

$$X_0^{\lambda\sigma} = \int \frac{d^2\boldsymbol{k}}{(2\pi)^2}\frac{2\pi e^2}{\epsilon k} F_{00}^{\lambda\lambda}(\boldsymbol{k})F_{00}^{\sigma\sigma}(-\boldsymbol{k})e^{ik_xk_y\ell^2}\mathcal{W}_X^{\lambda\sigma}, \quad (6)$$

$$Z_0^{\lambda\sigma} = U\int \frac{d^2\boldsymbol{k}}{(2\pi)^2} F_{00}^{\lambda\sigma}(\boldsymbol{k})F_{00}^{\sigma\lambda}(-\boldsymbol{k})e^{ik_xk_y\ell^2}\mathcal{W}_Z^{\lambda\sigma}, \quad (7)$$

where $\epsilon = (\epsilon_{\mathrm{SnTe}}+1)/2 \sim 20$ [31] is the effective dielectric constant and $F_{00}^{\lambda\sigma}(\boldsymbol{k})$ is a form factor that accounts for the system's valley-dependent cyclotron-orbit shape:

$$F_{00}^{\lambda\sigma}(\boldsymbol{k}) = \frac{\sqrt{2}}{\sqrt{|\alpha_\lambda||\alpha_\sigma|(\gamma_\lambda+\gamma_\sigma^*)}}\exp\left[\frac{(k_x^2+\gamma_\lambda\gamma_\sigma^* k_y^2)\ell^2}{-2(\gamma_\lambda+\gamma_\sigma^*)}\right]. \quad (8)$$

In the above integrals, $\mathcal{W}_X^{\lambda\sigma} = 1 - w_{\lambda\lambda} - w_{\sigma\sigma}$ and $\mathcal{W}_Z^{\lambda\sigma} = 1 - w_{\lambda\sigma} - w_{\sigma\lambda}$, with $w_{\lambda\sigma} = \gamma_\sigma^*/(\gamma_\lambda+\gamma_\sigma^*)$ and $\gamma_\lambda = \beta_\lambda/\alpha_\lambda$. If the surface states were isotropic (i.e., $v = v_x$ and $\gamma_\lambda = 1$), $F_{00}^{\lambda\sigma}(\boldsymbol{k})$ would reduce to the circular cyclotron-orbit form factor $\exp(-k^2\ell^2/4)$ [30]. The corrections in Eq. (8) account for the anisotropy of the triplet cyclotron orbits, and for the $2\pi/3$ differences in anisotropy orientation illustrated in Fig. 1, which play an essential role in the interaction physics. Because of the $\mathcal{C}_3$ symmetry, the intravalley exchange integral matrix $X_0^{\lambda\sigma}$ only has two inequivalent elements, stronger exchange integrals for electrons in the same valley (X_0^S) on its diagonal and weaker exchange integrals for electrons in different valleys (X_0^D) for its off-diagonal elements. Because we take the valley-exchange scattering to be short ranged, the intervalley integrals have only off-diagonal matrix elements, all of which have the same value (Y_0 and Z_0).

The broken symmetry ground state minimizes the total energy with respect to the five parameters that characterize the valley spinor, $(r_1e^{i\varphi_1}, r_2e^{i\varphi_2}, r_3)^{\mathrm{T}}$. Up to a spinor-independent constant, the energy per electron is

$$\mathcal{E} = 2[(X_0^S - X_0^D) - (Z_0 - Y_0)](r_1^2r_2^2 + r_2^2r_3^2 + r_3^2r_1^2). \quad (9)$$

The energy of the 1/3-filling ground state is independent of φ_1 and φ_2 because of separate particle number conservation in each valley. The spinor-dependent factor in Eq. (9) reaches its minimum value 0 when the spinor is a single-valley state $(r_1, r_2, r_3) = (1,0,0)$, (0,1,0), or (0,0,1) and its maximum value 1/3 when the ground state is an equal-weight three-valley state, $(r_1, r_2, r_3) = (1,1,1)/\sqrt{3}$.

Exchange energies are always stronger between orbitals that are more similar. Accordingly, the exchange integrals between electrons in the same valley are stronger than those between electrons in different valleys ($X_0^S > X_0^D > 0$) because of the difference in cyclotron-orbit orientations. It follows that the ground state is completely valley polarized unless valley-exchange interactions plays a role. LL interaction physics in SnTe surface 2DEGs therefore contrasts strongly with the case of graphene 2DEGs, which has identical isotropic Dirac cones in two different valleys, implying that $X_0^S = X_0^D$. Broken valley symmetry states at $\nu = \pm 1$ in graphene [32–35] therefore have Heisenberg character when valley-exchange processes are neglected.

For the relatively modest anisotropy parameter $\eta \sim 0.75$ of SnTe, we find that the difference between the same-valley and different-valley exchange energies is small, $X_0^S - X_0^D = 0.0541e^2/(\epsilon\ell) \sim \sqrt{B_\perp}$. The valley-exchange scattering processes are short ranged and momentum independent, under which $Z_0 - Y_0$ is positive and scales as $U/\ell^2 \sim B_\perp$. This allows the weak valley-exchange scattering to play a role at stronger fields, favoring a ground state which has coherence between all three valleys and is therefore a charge-density-wave state with broken translational symmetry. For $U = 2\pi e^2/\epsilon K = 0.85$ eV nm^2, a first-order quantum phase transition between nematic valley-polarized and valley-coherent charge-density-wave states occurs at $B_\perp^c \simeq 11$ T. This behavior contrasts with graphene [32–35] and monolayer MoS_2 [36], where there is no such competition, and the same mechanism induces a charge-density-wave ground state at all field strengths at filling factors $\nu = \pm 1$.

Zeeman-field effects.—We have so far neglected Zeeman coupling, which greatly enriches the interaction induced integer QH effect of SnTe. We write the total magnetic field as $(B_\parallel\cos\phi, B_\parallel\sin\phi, B_\perp)$, using the coordinate frame defined in Fig. 1(a) for the crucial in-plane-field orientation ϕ. For a general ϕ the Zeeman field breaks mirror symmetries and couples to the order parameter by producing valley-dependent single-particle energies [8,37], i.e., $E_0 \to E_0 + m_\lambda$ in Eq. (5), with

$$m_\lambda = \frac{1}{2}\alpha g\mu_B\left[\frac{2\sqrt{2}}{3}B_\parallel\cos(\phi-\theta_\lambda) + \frac{1}{3}B_\perp\right], \quad (10)$$

where g is an electron g factor, μ_B is the Bohr magneton, and $\alpha = \eta^2/3$ is the real spin weight of the surface pseudospin [8,37]. The perpendicular field $B_\perp$ does not break the $\mathcal{C}_3$ symmetry and contributes only an irrelevant

[38] valley-independent energy shift of the $N = 0$ triplet. In contrast, the in-plane field $B_\parallel$ breaks $\mathcal{C}_3$ symmetry and lifts the $N = 0$ triplet degeneracy. It follows that in-plane fields can yield an integer QH effect at the $1/3$ and $2/3$ fillings of the $N = 0$ triplet even in the absence of interactions, as illustrated in Fig. 2(a). When $\hat{B}_\parallel$ is parallel (antiparallel) to $\bar{\Gamma}$-$\bar{M}$, the triplet level degeneracy is reduced to a twofold degeneracy at $1/3$ ($2/3$) filling. When $\hat{B}_\parallel$ is (anti-)parallel to $\bar{\Gamma}$-$\bar{K}$, the single-particle gaps at the $1/3$ and $2/3$ fillings are nonzero and identical.

Valley-dependent Zeeman coupling competes with electron-electron interactions, and it greatly enriches the phase diagram by adding $\delta\mathcal{E} \to \sum_\lambda m_\lambda r_\lambda^2$ to Eq. (9). The phase diagram at $\epsilon g B_\parallel = 300$ T is illustrated in Fig. 2(b). For $B_\perp < B_\perp^c = (2.81\ \text{eV nm}^2/U)^2$, interactions prefer a valley-polarized state and ϕ simply selects which valley is occupied. First-order phase transitions occur at $\phi = \theta_\lambda$. When Zeeman coupling to a parallel field is included, the abrupt transition from valley-polarized to three-valley-coherent states is interrupted by a region in which ϕ-dependent two-valley-coherent states are stable. The stability range of the two-valley-coherent state is widest when $\phi = \theta_\lambda$. Finally, when $B_\perp$ is further increased, three-valley-coherent states finally emerge, but with ϕ-dependent and unequal valley populations. Valley coherence can therefore be modified and continuously tuned by the in-plane Zeeman field.

The shape of the phase diagram in Fig. 2(b) is only weakly dependent on the value of $\epsilon g B_\parallel$. The three first-order transition lines and $B_\perp^c$ are independent of

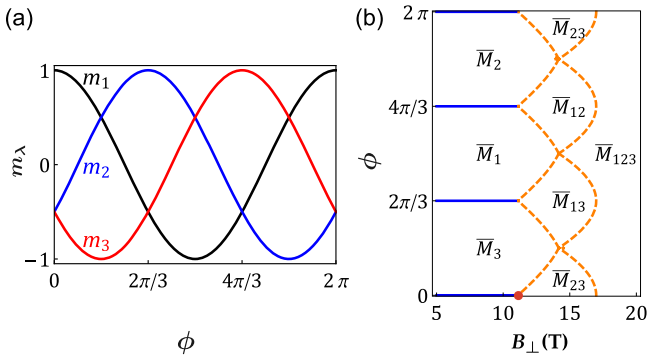

FIG. 2. (a) In-plane Zeeman energies m_λ in units of $\sqrt{2}\eta^2 g\mu_B B_\parallel/9$ as a function of $B_\parallel$ orientation. (b) Phase diagram for the state at $1/3$ filling of the $N = 0$ LL triplet for $\epsilon g B_\parallel = 300$ T and $U = 0.85$ eV nm^2. The red dot denotes the critical field $B_\perp^c$ at which a first-order transition occurs between a valley-polarized and a three-valley symmetric state occurs at $B_\parallel = 0$. The solid blue lines are first-order phase boundaries between valley-polarized states, and the dashed red lines are continuous transition boundaries between states with coherence between different numbers of valleys. The phases labeled by $\bar{M}_i$, $\bar{M}_{ij}$, and $\bar{M}_{123}$ have a full LL spinor that is a coherent superposition of components involving one, two, and three valleys, respectively.

changes in $\epsilon g B_\parallel$. A larger value of $\epsilon g B_\parallel$ expands the areas with two-valley-coherent states to larger $B_\perp$'s. Stronger short-range interactions shift $B_\perp^c$ to smaller values because intervalley interactions increase in importance. On the other hand, larger surface state anisotropy would increase the critical perpendicular field $B_\perp^c$.

Discussion.—We have shown that because of valley-dependent anisotropic cyclotron orbits, intravalley electron-electron interactions in SnTe can reduce rotational symmetries and lift the threefold degeneracy of the $\bar{M}$ valley $N = 0$ LLs. The physics which drives this broken symmetry is similar to that responsible for valley-polarized nematic states in parabolic spinful band systems with an even number of valleys [39,40]. The triplet case discussed here is distinguished by its SU(3) order parameter space, and by the way Zeeman interactions with parallel fields couple to the order parameter. Zeeman interactions play a key role because parallel fields break the mirror and $\mathcal{C}_3$ symmetries that protect and relate the three $\bar{M}$ valley surface Dirac states. We also predict that intervalley interactions will become important at sufficiently strong fields and drive a transition from a valley-polarized nematic state to a commensurate charge-density-wave state with intervalley coherence.

Although we use a mean-field theory, many of our predictions are exact when Landau-level mixing is neglected [41]. Specifically, the phase boundaries between the valley-polarized states (favored by in-plane Zeeman fields) and those between the valley-polarized and two-valley-coherent states are likely to be exact [41] because the states whose energies we are comparing are the only states in the relevant Hilbert space with the same quantum numbers. However, the phase boundaries between the two-valley-coherent states, which are not exact single-Slater determinant states, and the three-valley-coherent region are likely to be modified by quantum fluctuations.

The same physics also occurs in $Pb_xSn_{1-x}Se$, which may have higher mobilities than SnTe [4,42]. The first step experimentally would be to verify our predicted LL structure using field-angle dependent magnetoresistance or magnetic torque magnetometry [26,27]. The energies of the $\bar{\Gamma}$ and $\bar{M}$ valley LLs are $\sqrt{Nv^2 B_\perp}$ and $\sqrt{Nvv_x B_\perp}$, respectively. Their crossings, illustrated in Fig. 1, should lead to pronounced peaks in longitudinal magnetoresistance. Note that the LL crossing fields may be controllable by varying the surface potential [11], which tunes the energy difference between the $\bar{\Gamma}$ and $\bar{M}$ Dirac points. An in-plane Zeeman field splits the SU(3)-invariant triplets, with $2\pi/3$ periodicity as a function of Zeeman-field orientation. Since Shubnikov–de Haas oscillations have recently been observed on the (001) surface of $Pb_xSn_{1-x}Se$ [42], we expect future progress to be rapid. The phase diagram Fig. 2(b) is expected to be observable only in low-disorder samples since the transport activation gaps associated with broken symmetry states are of the order of

$e^2/(\epsilon\ell) \sim 56\sqrt{B_\perp[\mathrm{T}]}/\epsilon$ meV. The collective modes [43] of valley-coherent states are expected to be gapless, while those of valley-polarized states are expected to be gapped.

We thank Qian Niu for the helpful discussions. X. L. was supported by the U.S. DOE (Grant No. DE-FG03-02ER45958, Division of Materials Science and Engineering) and the Welch Foundation (Grant No. F-1255) in Austin, Texas, and is currently supported by JQI-NSF-PFC and LPS-MPO-CMTC in Maryland. F. Z. is supported by the University of Texas at Dallas research enhancement funds. F. Z. also thanks the Aspen Center for Physics (NSF Grant No. 1066293 and the Trustees Fund) for its hospitality during the finalization of this work. A. H. M. is supported by U.S. DOE Division of Materials Sciences and Engineering Grant No. DE-FG02-02ER45958, and by Welch Foundation Grant No. TBF1473.

*zhang@utdallas.edu

[1] D. L. Mitchell and R. F. Wallis, Phys. Rev. **151**, 581 (1966).
[2] T. H. Hsieh, H. Lin, J. Liu, W. Duan, A. Bansil, and L. Fu, Nat. Commun. **3**, 982 (2012).
[3] Y. Tanaka, Z. Ren, T. Sato, K. Nakayama, S. Souma, T. Takahashi, K. Segawa, and Y. Ando, Nat. Phys. **8**, 800 (2012).
[4] P. Dziawa, B. J. Kowalski, K. Dybko, R. Buczko, A. Szczerbakow, M. Szot, E. Lusakowska, T. Balasubramanian, B. M. Wojek, M. H. Berntsen, O. Tjernberg, and T. Story, Nat. Mater. **11**, 1023 (2012).
[5] S. Xu *et al.*, Nat. Commun. **3**, 1192 (2012).
[6] S. Safaei, P. Kacman, and R. Buczko, Phys. Rev. B **88**, 045305 (2013).
[7] J. Liu, W. Duan, and L. Fu, Phys. Rev. B **88**, 241303(R) (2013).
[8] F. Zhang, X. Li, J. Feng, C. L. Kane, and E. J. Mele, arXiv:1309.7682.
[9] Y. Tanaka, T. Shoman, K. Nakayama, S. Souma, T. Sato, T. Takahashi, M. Novak, K. Segawa, and Y. Ando, Phys. Rev. B **88**, 235126 (2013).
[10] J. Wang, J. Liu, Y. Xu, J. Wu, B. L. Gu, and W. Duan, Phys. Rev. B **89**, 125308 (2014).
[11] Y. Shi, M. Wu, F. Zhang, and J. Feng, Phys. Rev. B **90**, 235114 (2014).
[12] S. Safaei, M. Galicka, P. Kacman, and R. Buczko, New J. Phys. **17**, 063041 (2015).
[13] J. Liu and L. Fu, Phys. Rev. B **91**, 081407 (2015).
[14] X. Li, B. Roy, and S. D. Sarma, Phys. Rev. B **92**, 235144 (2015).
[15] S. L. Sondhi, A. Karlhede, S. A. Kivelson, and E. H. Rezayi, Phys. Rev. B **47**, 16419 (1993).
[16] M. Rasolt, F. Perrot, and A. H. MacDonald, Phys. Rev. Lett. **55**, 433 (1985).
[17] K. Moon, H. Mori, K. Yang, S. M. Girvin, A. H. MacDonald, L. Zheng, D. Yoshioka, and S.-C. Zhang, Phys. Rev. B **51**, 5138 (1995).
[18] I. B. Spielman, J. P. Eisenstein, L. N. Pfeiffer, and K. W. West, Phys. Rev. Lett. **84**, 5808 (2000).
[19] M. Shayegan, E. P. De Poortere, O. Gunawan, Y. P. Shkolnikov, E. Tutuc, and K. Vakili, Phys. Status Solidi B **243**, 3629 (2006).
[20] B. E. Feldman, J. Martin, and A. Yacoby, Nat. Phys. **5**, 889 (2009).
[21] Y. Zhao, P. Cadden-Zimansky, Z. Jiang, and P. Kim, Phys. Rev. Lett. **104**, 066801 (2010).
[22] Y. Lee, J. Velasco, Jr., D. Tran, F. Zhang, W. Bao, L. Jing, K. Myhro, D. Smirnov, and C. N. Lau, Nano Lett. **13**, 1627 (2013).
[23] F. Zhang, D. Tilahun, and A. H. MacDonald, Phys. Rev. B **85**, 165139 (2012).
[24] K. Eng, R. N. McFarland, and B. E. Kane, Phys. Rev. Lett. **99**, 016801 (2007).
[25] T. M. Kott, B. Hu, S. H. Brown, and B. E. Kane, Phys. Rev. B **89**, 041107 (2014).
[26] L. Li, J. G. Checkelsky, Y. S. Hor, C. Uher, A. F. Hebard, R. J. Cava, and N. P. Ong, Science **321**, 547 (2008).
[27] Z. Zhu, A. Collaudin, B. Fauqué, W. Kang, and K. Behnia, Nat. Phys. **8**, 89 (2012).
[28] S. A. Kivelson, E. Fradkin, and V. J. Emery, Nature (London) **393**, 550 (1998).
[29] F. Zhang, C. L. Kane, and E. J. Mele, Phys. Rev. B **86**, 081303 (2012).
[30] R. Côté and A. H. MacDonald, Phys. Rev. B **44**, 8759 (1991).
[31] H. R. Riedl, J. R. Dixon, and R. B. Schoolar, Phys. Rev. **162**, 692 (1967).
[32] K. Nomura and A. H. MacDonald, Phys. Rev. Lett. **96**, 256602 (2006).
[33] M. O. Goerbig, R. Moessner, and B. Douçot, Phys. Rev. B **74**, 161407 (2006).
[34] J. Alicea and M. P. A. Fisher, Phys. Rev. B **74**, 075422 (2006).
[35] K. Yang, S. Das Sarma, and A. H. MacDonald, Phys. Rev. B **74**, 075423 (2006).
[36] X. Li, F. Zhang, and Q. Niu, Phys. Rev. Lett. **110**, 066803 (2013).
[37] F. Zhang, C. L. Kane, and E. J. Mele, Phys. Rev. Lett. **110**, 046404 (2013).
[38] Note that the Zeeman effects of $B_\perp$ are distinct [8] for $\bar{\Gamma}$ and $\bar{M}$ states.
[39] D. A. Abanin, S. A. Parameswaran, S. A. Kivelson, and S. L. Sondhi, Phys. Rev. B **82**, 035428 (2010).
[40] A. Kumar, S. A. Parameswaran, and S. L. Sondhi, Phys. Rev. B **88**, 045133 (2013).
[41] J. Schliemann and A. H. MacDonald, Phys. Rev. Lett. **84**, 4437 (2000).
[42] Y. Okada, M. Serbyn, H. Lin, D. Walkup, W. Zhou, C. Dhital, M. Neupane, S. Xu, Y. Wang, R. Sankar, F. Chou, A. Bansil, M. Z. Hasan, S. D. Wilson, L. Fu, and V. Madhavan, Science **341**, 1496 (2013).
[43] I. B. Spielman, J. P. Eisenstein, L. N. Pfeiffer, and K. W. West, Phys. Rev. Lett. **87**, 036803 (2001).

SU(3) Quantum Hall Ferromagnetism in SnTe

Citation:

Li, X., F. Zhang, and A. H. MacDonald. 2016. "SU(3) quantum hall ferromagnetism in SnTe." Physical Review Letters 116(2), doi:10.1103/PhysRevLett.116.026803.